Molecular motors in new media

Lubbe, Anouk Sophia

Chapter 3: Light Actuated Morphological Change in Organic Microcrystals

The development of dynamic responsive molecular systems is an ongoing quest in many disciplines of chemistry. In crystal engineering, the search for a trigger that can elicit response is especially challenging, since crystalline materials are often solids. In this chapter, a first generation molecular motor functionalized with thymine substituents is designed and developed. After characterization of the rotational properties of this motor, using NMR and UV-vis spectroscopy, the motor is used to create a responsive crystalline material. Using a combination of Transmission Electron Microscopy and UV-vis spectroscopy, it is demonstrated that the crystalline material formed by the motor can be broken up in smaller pieces by rotation of the motor.

This work will be submitted for publication. Manuscript in preparation.

3.1 Introduction

Crystal engineering has emerged as an important field of materials sciences, in which new materials are designed based on an understanding of the intermolecular forces between the molecules that make up the compounds.[1] Through the study of large sets of crystalline materials, specific intermolecular interactions may be linked to material properties, allowing scientists to predict and understand behaviour of new materials that can be crystalline.[2–7]

For many years, the process of growing crystals was a metaphorical "black box".[8] Specific supramolecular interactions governing the makeup of a crystalline material could only be discovered after synthesis of the building block and subsequent crystallization. Although chemists have tried discovering trends in molecular determinants of crystal structures for many years, the size of the available data sets has been a historical limiting factor in creating reliable predictions.[1] However, the recent abundant availability of data has contributed to exponential growth in crystal engineering research.[9] Additionally, the increasing interest in this field reflects a general trend in chemical science, focusing on supramolecular systems and collective behaviour, opposed to single molecule dynamics.[10]

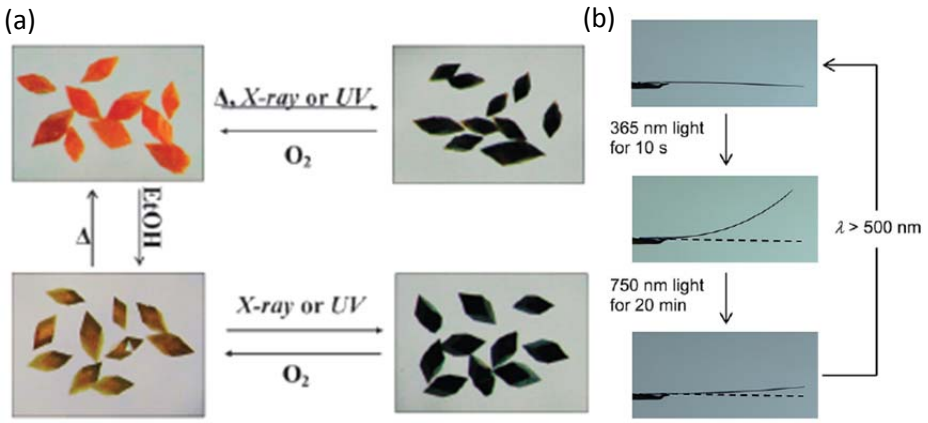

Figure 3.1: Two striking examples of photoregulation of crystalline materials. (a) A stable, viologen cation containing MOF. The photochemically induced colour change can be reversed by exposure to oxygen. Reproduced with permission from ref. 19, Royal Society of Chemistry 2013. (b) Light-driven bending of a diarylethene containing crystal. Reproduced with permission from ref. 18, Royal Society of Chemistry 2015.

One of the advantages of supramolecular systems is that they can be highly responsive. For example, a dynamic covalent library is in continuous equilibrium, and can be modified in a myriad of ways by the simple addition of a single building block.[11,12] Since solid crystalline materials are essentially static, there is an ongoing search for triggers that would elicit dynamic response in material properties. A particular interest has aris-

en for the use of light to modify crystalline solid properties, since it is non-invasive and allows for a high level of spatiotemporal control.[13–18]

Light responsiveness on the molecular level may be achieved using photoswitches, which are small molecules that undergo a reversible geometric change upon irradiation. Among the molecular photoswitches, overcrowded alkene-based rotary motors hold a special position, since they can assume four different states in their rotary cycle. [13,20,21] Additionally, their core structure is helical and the helicity is inversed in each switching step. This unique property has already been used in the past to drive the unidirectional rotation of a microscale object.[22] For a more detailed description of molecular motors and their rotary properties, see Chapter 2.

Molecular motors are robust photoresponsive systems and have been used in a range of applications.[21,23] We considered it therefore likely that, as with other photoswitches, molecular motors may be used to exert photocontrol over the structure of a crystalline supramolecular aggregate. Moreover, we were intrigued to see whether the possibility of addressing multiple states and the accompanying helix inversions would allow us to reach a higher level of precision in controlling the structure of the material.

Typically, overcrowded alkene-based molecular motors are crystalline materials. For the current design, we aimed to incorporate functional groups that are able to form additional noncovalent binding interactions. If one such functional group is positioned on each half of the motor, photoswitching will lead to a relative change in orientation of these moieties. As a result, supramolecular interactions may be altered or newly formed. This concept has already been successfully applied to create a photoresponsive bilayer,[24] photoswitchable anion receptors[25] and photoswitchable gelators.[26]

For our molecular design, we decided to rely on hydrogen bonding to control interactions between molecules. Hydrogen bonding represents a highly predictable noncovalent binding interaction. The traditional Pauling hydrogen bond is quite strong, typically ranging from 15-30 kJ/mol, but can reach values up to 160 kJ/mol (for $F\text{-}H\cdots F^-$).[3] Recently, IUPAC has broadened the definition of a hydrogen bond to any electrostatic interaction between a hydrogen atom and another, more electronegative atom, thus also including weaker (and stronger) interactions (5-15 kJ/mol).[27] Hydrogen bonding is used extensively in crystal engineering, and has found real promise in the development of porous networks which may be used for storage and separation of gases.[28–30]

In order to utilize hydrogen bonding in the formation of a photoresponsive crystalline material, we chose to functionalize a first generation molecular motor with thymine groups. Thymine-thymine interactions are weaker than thymine-adenine interactions but can exist in naturally occurring oligonucleotides.[31] Additionally, thymine is a cyanuric acid analogue, and can be used for self-assembly with melamine.[32] Melamine-cyanuric acid lattices were first described in 1990,[33] and have since been investigated in

detail.[34–36] We envisioned that a thymine functionalized motor may be used to form photocontrollable supramolecular assemblies on its own or with melamine.

3.2 Synthesis

Carboxylic acid-functionalized motor **3.1**[37,38] and 2-aminoethane-functionalized thymine **3.2**[39] were synthesized according to literature procedures. Benzotriazol-1-yl-oxytripyrrolidinophosphonium hexafluorophosphate (PyBOP) mediated[40] double coupling of *trans*-**3.1** and **3.2** yielded *trans* thymine functionalized motor **3.3** (see Scheme 3.1). Coupling of *cis*-**3.1** and **3.2** was unsuccessful, but *cis*-**3** could be obtained by irradiation. Irradiating *trans*-**3.3** with λ = 312 nm light for several hours (stable *trans* to unstable *cis* isomerization), led to the formation of a PSS consisting of 70% unstable *cis*-**3.3**. Subsequently, heating to 40 °C caused a thermal helix inversion from unstable to stable *cis* with full conversion. Finally, the isomers could be separated *via* flash column chromatography.

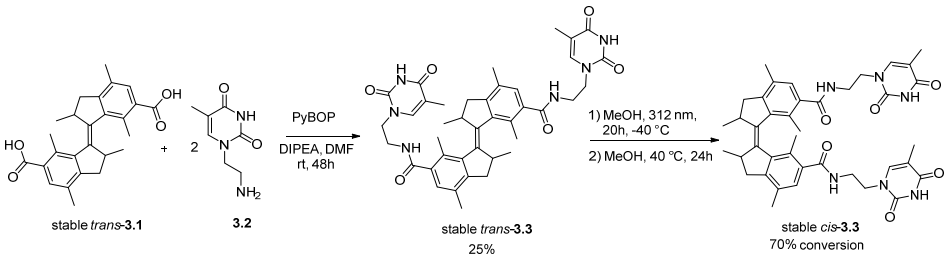

Scheme 3.1: Synthesis of thymine functionalized motor **3.3**.

3.3 Analysis of photochemical properties of motor **3.3**.

3.3.1 NMR analysis

The thermal and photochemical steps in the rotation of molecular motor **3.3** were studied using ^{1}H-NMR spectroscopy. Figure 3.2i shows the ^{1}H NMR spectrum of stable *trans*-**3.3** in DMF-d7. The sample was cooled to –40 °C and irradiated with 312 nm light. The photostationary state (PSS, Figure 3.2ii) was reached after 15 h and consists of a stable *trans*/unstable *cis* ratio of 17:83. Unstable *cis*-**3.3** was fully converted to stable *cis*-**3.3** by heating the sample to 40 °C for 24 h (Figure 3.2iii).

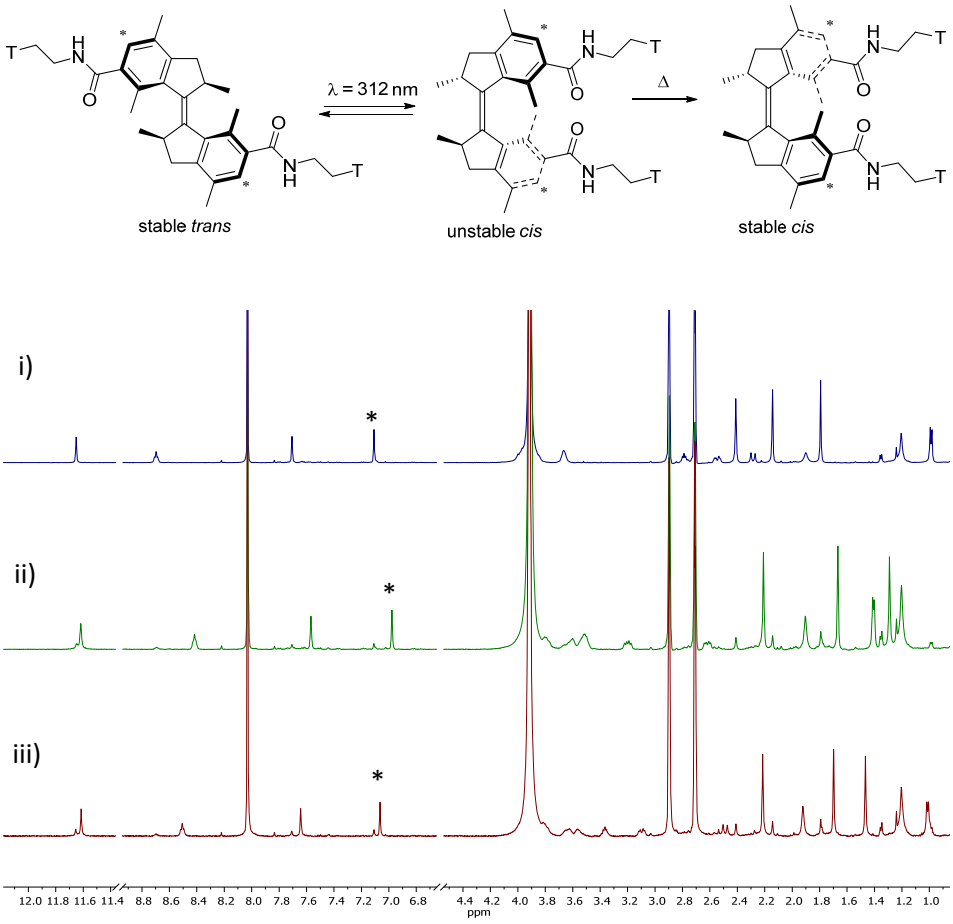

Figure 3.2: NMR experiments in DMF-d7 (400 MHz, –40 °C). i) Stable *trans*-**3.3**, ii) PSS, reached after 15 h of irradiation (312 nm, –40 °C), iii) Sample after heating to 40 °C for 24 h, consisting mainly of stable *cis*-**3.3**. T = thymine. * Indicates the aromatic proton on the motor unit.

Figure 3.3i shows the NMR spectrum of stable *cis*-**3** in DMF-d7. The sample was cooled to –40 °C and irradiated with 312 nm light. The photostationary state (PSS, Figure 3.3ii) was reached after 7 h and consists of a stable *cis*/unstable *trans* ratio of 9:91, as well as a small amount of stable *trans* and unstable *cis*. Unstable *trans*-**3.3** was fully converted to stable *trans*-**3.3** by heating the sample to rt for 10 min (Figure 3.3iii).

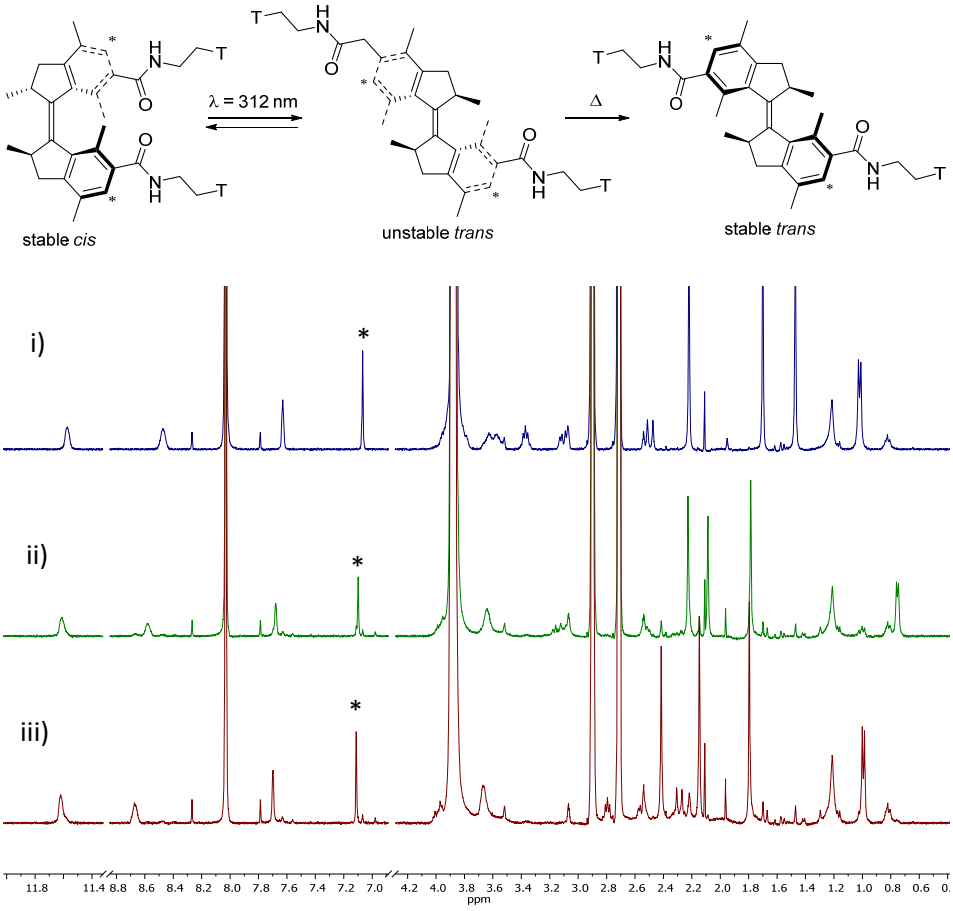

Figure 3.3: NMR experiments in DMF-d7 (400 MHz, –40 °C). i) Stable *cis*-**3.3**, ii) PSS, reached after 7 h of irradiation (312 nm, –40 °C), iii) Sample after heating to rt for 10 min, consisting mainly of stable *trans*-**3.3**. T = thymine. * Indicates the aromatic proton on the motor unit.

3.3.2 UV-vis analysis

The photochemical properties of motor **3.3** were studied using UV-vis spectroscopy. A $2 \cdot 10^{-5}$ M solution of motor *trans*-**3.3** was prepared in methanol and a UV-vis spectrum was recorded (Figure 3.4). The sample was irradiated with 312 nm light at 20 °C. Spectra were recorded at regular intervals (Figure 3.4a). The irradiation caused the major absorption band (λ_{max} = 278 nm) to decrease. Simultaneously, a new band appeared at 345 nm. This bathochromic shift is in accordance with formation of a higher energy isomer (unstable *cis*-**3.3**). The clear isosbestic point at 319 nm is indicative of the absence of undesired side reactions. After 45 min, a photostationary state was reached (Figure 3.4b). Upon removal of the light source and heating to 50 °C for several hours, the band centered around 345 nm completely disappeared, and an increase of the absorption at lower wavelengths was observed. This obervation indicates that the thermal helix inversion was completed, and the sample contained a mixture of stable *trans*-**3.3** and stable *cis*-**3.3**. This conclusion is supported by the ^{1}H NMR analysis.

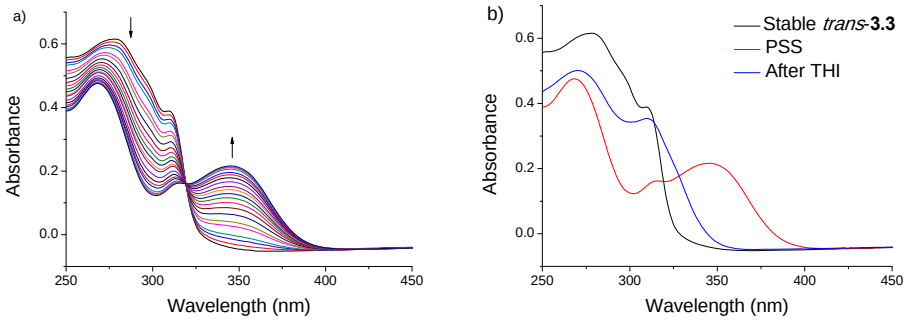

Figure 3.4: UV-vis spectra of analysis of the photochemical isomerization and subsequent thermal helix inversion of stable *trans*-**3.3**. (a) Changes of the absorption spectrum of stable *trans*-**3.3** upon irradiation with 312 nm light. (b) UV-vis spectra of stable *trans*-**3.3** (black line), the photostationary state (red line) and the sample after the thermal helix inversion (blue line). All spectra recorded in methanol.

To study the other half of the rotational cycle, a $2 \cdot 10^{-5}$ M solution of motor cis-**3.3** was prepared in methanol and a UV-vis spectrum was recorded (Figure 4.5). The sample was irradiated with 312 nm light at -20 °C. Spectra were recorded at regular intervals (Figure 4.5a). The irradiation caused the major absorption band (λ_{max} = 271 nm) to decrease. Simultaneously, two new bands appeared at 266 nm and 327 nm. The bathochromic shift is in accordance with formation of a higher energy isomer (unstable *trans*-**3.3**). An isosbestic point was observed around 317 nm, but started shifting slightly after several minutes. This shift is most likely due to thermal helix inversion occurring to form stable *trans*-**3.3**, and further photochemical *trans-cis* isomerization towards unstable *cis*-**3.3**. These processes might be eliminated by performing the irradiation at a lower temperature, which in the current experiment was impossible due to the temperature limits of the setup. After 13 min, the irradiation was stopped (Figure 4.5b). Upon removal of the light source and heating to room temperature for 30 min, the band centered around 327 nm significantly decreased, and an increase of the absorption at lower wavelengths was observed. This obervation indicates that the thermal helix inversion of unstable *trans*-**3.3** towards stable *trans*-**3.3** was completed, and the sample contained a mixture of mainly stable *trans*-**3.3** and stable *cis*-**3.3**. A small red-shifted band indicates the presence of a small amount unstable *cis*-**3.3**, which has a half life of several days at room temperature. These conclusions are supported by ^{1}H NMR analysis.

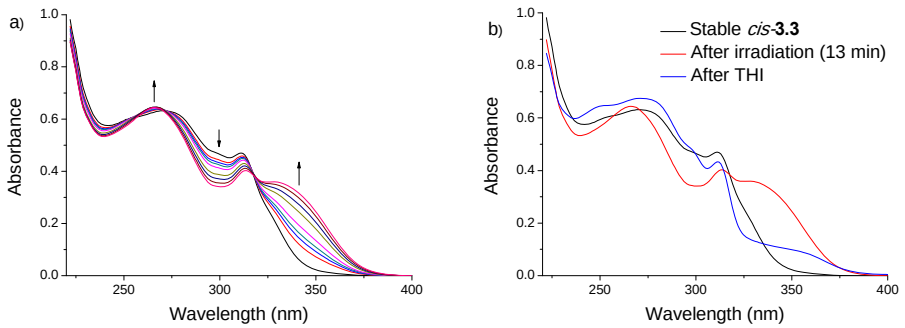

Figure 3.5: UV-vis spectra of analysis of the photochemical isomerization and subsequent thermal helix inversion of stable *cis*-**3.3**. (a) Changes of the absorption spectrum of stable *cis*-**3.3** upon irradiation with 312 nm light. (b) UV-vis spectra of stable *cis*-**3.3** (black line), the spectrum after 13 minutes of irradiation (red line) and the sample after the thermal helix inversion (blue line).

3.3.3 Kinetic analysis

A $2 \cdot 10^{-5}$ M solution of motor **3.3** was prepared in methanol and the solution was purged with argon. Samples were prepared in quartz cuvettes (l = 1.0 cm). The samples were irradiated with 312 nm light at 20 °C, until the photostationary state was reached. The absorption at 350 nm was then measured over time until the thermal process was complete. A 320 nm cut-off filter was mounted in front of the light source to minimize photochemical conversion occurring during the thermal helix inversion. All exponential decay lines were fitted using least squares approach. The results were processed using a direct Eyring analysis with error margins obtained by a Monte Carlo experiment. Table 3.1 lists the activation parameters and half lives determined for both processes. The Eyring plots are depicted in Figure 3.6.

	$t_{1/2}$ at 20 °C	$\Delta^{\ddagger}G°$ (kJ/mol)	$\Delta^{\ddagger}H°$ (kJ/mol)	$\Delta^{\ddagger}S°$ (J/K/mol)
Unstable *trans* to stable *trans*	14 s ± 2.7	79.0 ± 0.5	85.3 ± 3.4	21.5 ± 13.2
Unstable *cis* to stable *cis*	60 h ± 5	102.6 ± 0.2	97.1 ± 2.1	-18.7 ± 6.5

Table 3.1: Activation parameters and half-lives calculated for both isomers of motor **3.3**.

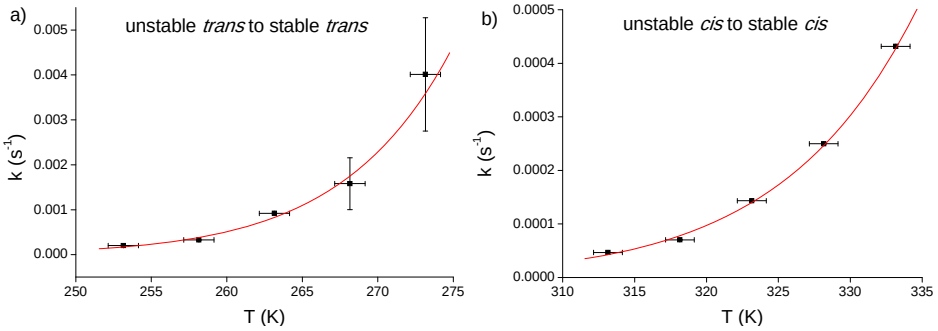

Figure 3.6: Eyring plots for the thermal helix inversions of motor **3.3**. (a) Unstable *trans*-**3.3** to stable *trans*-**3.3**. (b) Unstable *cis*-**3.3** to stable *cis*-**3.3**.

3.4 CPD formation

Cyclo-butyl pyrimidine dimer (CPD) formation in DNA is one of the leading causes of skin cancer.[41] Irradiation with UV light can cause [2+2] cycloaddition of adjacent thymine moieties. The resulting CPD can lead to mismatches and translation errors. Since the irradiation wavelength of xylene-based first generation motors (312 nm) falls within the range of UV-B light, motor **3.3** may be susceptible to CPD formation. Photodimerization is a particular risk for the *cis* isomers, in which the thymine moieties are placed in close proximity. This possibility was investigated using a model compound, and subsequently using motor **3.3** itself. From these experiments, it became evident that motor **3.3** is not at risk for photoinduced CPD formation. It seems likely that rapid

energy transfer to the aromatic core of the motor inhibits the photodimerization processes. The full experiment may be found in reference 42.

3.5 TEM experiments

Following the control experiments the key investigation was started, which aimed at creating a photoresponsive crystalline material. Molecular motor *trans*-**3.3** was dissolved in DCM. From this stock solution, a volume equating to ~1 µmol of motor was taken and film dried in a vial under a N_2 flow. Subsequently, 1.0 mL of a 2/1 (v/v) water/ethanol mixture was added. The vials were then vortexed for ~1 min, and subsequently sonicated for ~5 min. After this preparation, an opaque solution was obtained, without any visible precipitate. The mixture was analysed using transmission electron microscopy (TEM). Elongated hexagonal sheets could be observed in the sample prepared from *trans*-**3.3** (Figure 3.9a1). The sheets are typically 1.5-5 µm wide and up to 15 µm long. Subsequently, an identical sample was prepared, containing additionally 1.0 eq of melamine. Surprisingly, identical results were obtained from TEM analysis (Figure 3.7). Melamine by itself prepared under the same conditions shows no discernible features in TEM. Therefore, it seems likely that motor **3.3** forms these microcrystalline sheets only by itself, and that they are thermodynamically more stable than any potential motor-melamine adduct.

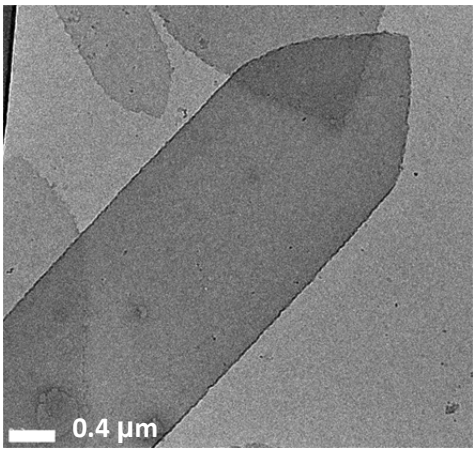

Figure 3.7: TEM image of melamine containing sample: 1/1 *trans*-**3.3**/melamine in 2/1 water/ethanol.

Electron diffraction experiments confirmed that the hexagonal sheets are crystalline (Figure 3.8a). Energy dispersive X-ray spectroscopy (EDX) showed that nitrogen is abundantly present in the sheets, while virtually no nitrogen is present elsewhere on the grid surface (Figure 3.8b).

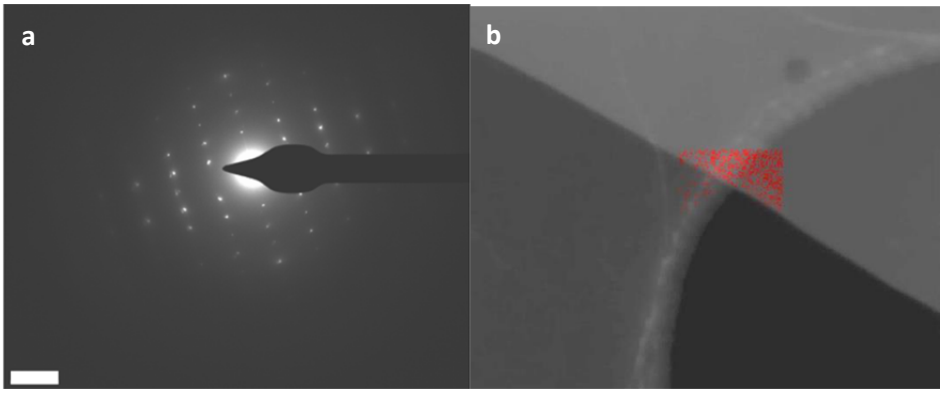

Figure 3.8: TEM images of *trans*-**3.3** and 1 eq. of melamine in 2/1 water/ethanol. (a) Electron diffraction performed on a hexagonal crystal. (b) EDX mapping (nitrogen) of crystal on carbon surface.

In addition to the TEM imaging (Figure 3.9a1), the sample (containing *trans*-**3.3** in 2/1 water/ethanol) was also analysed using UV-vis spectroscopy. An aliquot was removed from the sample, dissolved in dichloromethane and a UV-vis spectrum was recorded. As expected, the UV-vis spectrum of the initial sample (stable *trans*-**3.3** in 2/1 water/ethanol, vortexed and sonicated, small aliquot dissolved in DCM, Figure 3.9a2, black line) looks almost identical to the UV-vis spectrum of stable *trans*-**3.3** recorded in methanol (Figure 3.9a2, red line).

Subsequently, the sample was irradiated for 1 h using 312 nm light, to form the unstable *cis* isomer, and again examined using TEM. Interestingly, most of the regular hexagonal sheets had disappeared. Figure 3.9b1 shows one typical image recorded of the sample. A hexagonal structure is still clearly discernible on the right. The structure on the left is much more irregular, and smaller sheets can also be observed. Several images of the sample show hexagonal sheets which appear partly broken down. Figure 3.9b2 (black line) shows the UV-vis spectrum of this sample. A new band has appeared with a maximum absorption at 345 nm. This band overlaps perfectly with the band corresponding to the unstable *cis* isomer of motor *trans*-**3.3** at PSS in methanol (Figure 3.9b2, red line).

Finally, the sample was subjected to heating to 50 °C for 16 h, to promote the relaxation from unstable *cis* to stable *cis* isomer. After the heating, no more hexagonal crystalline sheets were observed. Instead, the sample seemed to contain mainly stacked sheets, some of which appear to be rectangular (Figure 3.9c1). These structures are notably smaller (< 0.5 x 0.5 µm) than the hexagonal sheets that can be seen in Figure 3.9a1. In the UV-vis spectrum, the heating step caused the new band observed after irradiation to decrease (Figure 3.9c2, black line). The disappearance of this band is in accordance with the thermal helix inversion from the unstable *cis*-**3.3** isomer to stable *cis*-**3.3** (Figure 3.9c2, red line).

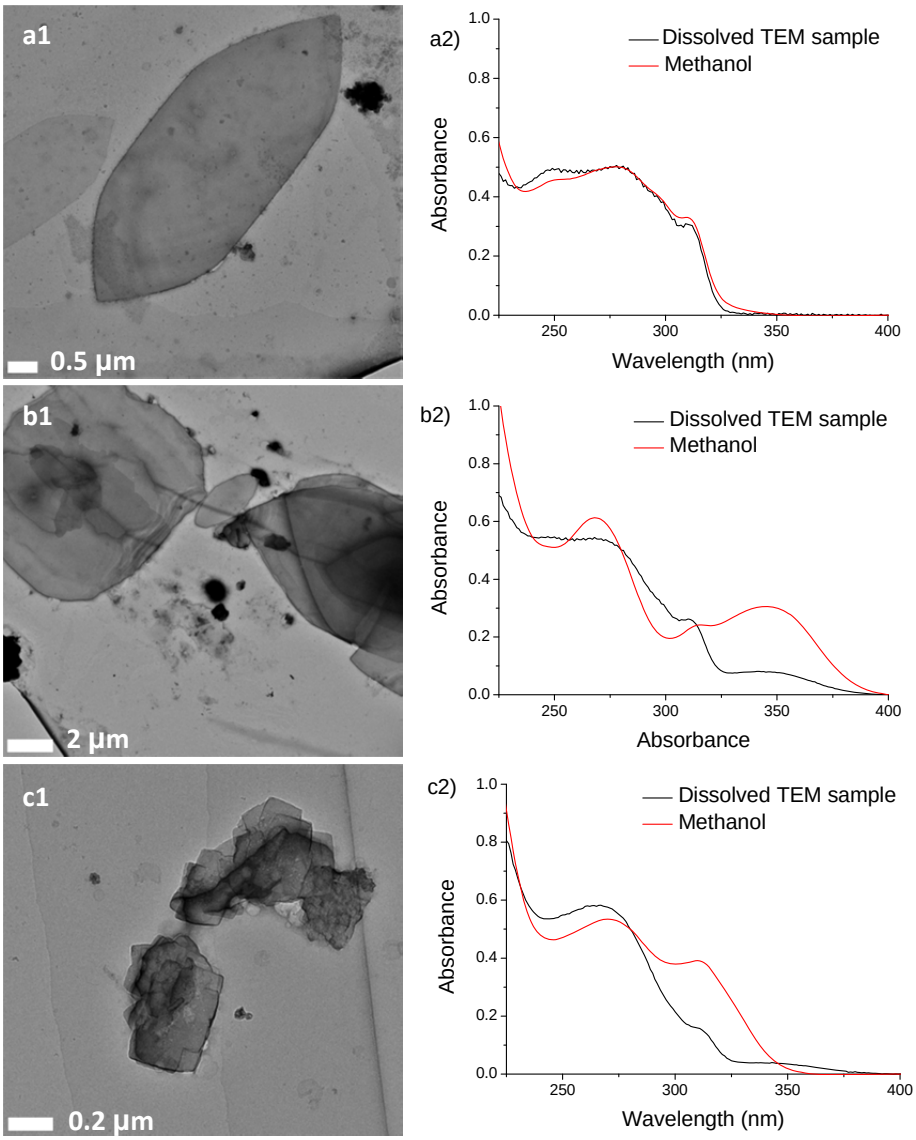

Figure 3.9: TEM images and UV-vis spectra of *trans*-**3.3** in 2/1 water/ethanol. (1) TEM images, (2) UV-vis spectra of TEM samples (*trans*-**3.3** in 2/1 water/ethanol, dissolved in dichloromethane, black lines), and stable *trans*-**3.3** dissolved in methanol for reference (red lines). (a) *Trans*-**3.3**. (b) After irradiation with 312 nm light. (c) After heating to 50 °C, 16 h. All UV-vis spectra normalized to allow comparison.

Judging by the UV-vis spectra displayed in Figure 3.9a2-c2, motor *trans*-**3.3** in the aggregated state appears to undergo rotary motion upon irradiation and subsequent heating in the TEM sample. As a reference, a sample of *cis*-**3.3** was prepared using the same procedure and analysed using TEM (Figure 10). Although this sample also appeared to be crystalline in nature, these needle-like crystals did not bear any resem-

blance to the structures observed in Figure 3.9c1. However, sample c consists of a mixture of isomers and it is therefore not surprising that no well-defined aggregates are formed.

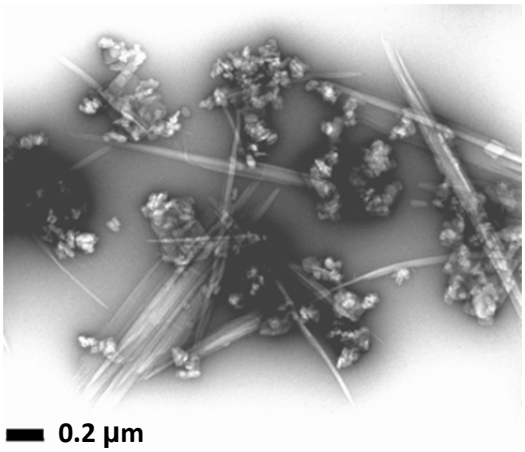

Figure 10: TEM image of cis-**3.3** in 2/1 water/ethanol.

3.6 Conclusions

In comparison with motor **3.3** in solution (Figure 3.9a2-c2, red lines), the rotational process in the water/ethanol sample is less efficient. Due to the crystalline nature of the sample, the motor movements may be more restricted. It has been demonstrated several times that rotation of molecular motors can be achieved in gels,[26,43] but in fact, motor rotation in the solid state has not yet been reported. The TEM images reported here clearly suggest that the breaking of the crystalline sheets is the result of motor rotation. Comparison of the crystalline sample with a fully dissolved motor indicates that the aggregated motor undergoes the often reported unidirectional rotation process.

Moreover, this unprecedented result illustrates the power of overcrowded alkene based molecular motors. Most molecular motors are crystalline, and although their solid state switching has not been observed previously, it seems likely that more light-driven rotary molecular motors are able to overcome the restrictions of the crystal lattice. The experiments reported herein mainly serve as a proof-of-principle of unidirectional rotation in crystal structure on a molecular scale. However this discovery may be highly useful in the design of responsive crystalline materials.

3.7 Experimental procedures and acknowledgements

For general remarks, see Chapter 2. TEM experiments were conducted by dr. Marc Stuart and Petra Erne. The synthesis and characterization of motor **3.3** were previously reported, and were performed under the guidance of dr. Nopporn Ruangsupapichat.[42] However, the synthesis was subsequently optimized and the route reported herein is different than previously reported. Additionally, UV-vis and NMR analysis of the rotary cycle of **3.3** were repeated for this thesis, because a higher purity of the material was achieved.

(*E*)-2,2',4,4',7,7'-hexamethyl-*N*6,*N*6'-bis(2-(5-methyl-2,4-dioxo-3,4-dihydropyrimidin-1(2*H*)-yl)ethyl)-2,2',3,3'-tetrahydro-[1,1'-biindenylidene]-6,6'-dicarboxamide (*trans*-3.3)

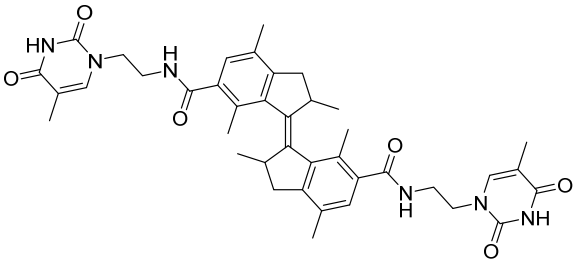

Carboxylic acid-functionalized motor *trans*-**3.1**[38] (91 mg, 0.23 mmol), aminoethane functionalized thymine **3.2**[39] (84 mg, 0.50 mmol) and PyBOP (240 mg, 0.45 mmol) were mixed in a round bottom flask under a N_2 atmosphere. DMF (1 mL) and di-*iso*-propyl-ethylamine (220 µL, 160 mg, 1.2 mmol) were added and the mixture was stirred at room temperature for 16 h. The reaction mixture was evaporated on celite and purified by column chromatography (SiO_2, MeOH/H_2O/DMSO/NEt_3 8:2:0.1:0.1 to 0:10:0.1:0.1). Thymine-functionalized motor *trans*-**3.3** was obtained as a white powder (31 mg, 0.06 mmol, 25%). ^{1}H NMR (400 MHz, DMSO-d6) δ 11.21 (s, 2H), 8.35 (t, *J* = 6.0 Hz, 2H), 7.47 (s, 2H), 6.99 (s, 2H), 3.92 – 3.68 (m, 4H), 3.49 (m, 4H), 2.78 (app p, 2H), 2.55 (dd, *J* = 15.3, 6.1 Hz, 2H), 2.32 (s, 6H), 2.26 (d, *J* = 14.8 Hz, 2H), 2.16 (s, 6H), 1.75 (s, 6H), 1.01 (d, *J* = 6.3 Hz, 6H); ^{13}C NMR (101 MHz, DMSO-d6) δ 169.8, 164.5, 151.0, 142.9, 142.1, 141.2, 141.0, 136.4, 130.6, 128.1, 127.3, 107.8, 47.5, 41.5, 38.4, 37.4, 19.4, 18.8, 17.8, 11.9; HRMS (ESI): *m/z* calcd for $C_{40}H_{47}N_6O_6$ ($M+H^+$): 707.35516, found 707.35410.

(*Z*)-2,2',4,4',7,7'-hexamethyl-*N*6,*N*6'-bis(2-(5-methyl-2,4-dioxo-3,4-dihydropyrimidin-1(2*H*)-yl)ethyl)-2,2',3,3'-tetrahydro-[1,1'-biindenylidene]-6,6'-dicarboxamide (*cis*-3.3)

Trans-**3.3** was dissolved in methanol and the solution was purged with argon. The solution was cooled to -40 °C and irradiated with 312 nm light for 20 h to induce photoisomerization, and subsequently heated to 40 °C to induce thermal helix inversion. The two isomers could be separated by column chromatography (SiO_2, MeOH/H_2O/DMSO/NEt_3 8:2:0.1:0.1 to 0:10:0.1:0.1). Thymine-functionalized motor *cis*-**3** was obtained as a white powder. ^{1}H NMR (500 MHz, DMF-d7) δ 11.16 (s, 2H), 8.16 (t, *J* = 6.0 Hz, 2H), 7.52 (s, 2H), 7.09 (s, 2H), 4.04 – 3.82 (m, 4H), 3.64 (m, 4H), 3.41 (app p, 2H), 3.14 (dd, *J* = 15.4, 6.3 Hz, 2H), 2.53 (d, *J* = 15.4 Hz, 2H), 2.26 (s, 6H), 1.73 (s, 6H), 1.51 (s, 6H), 1.07 (d, *J* = 6.7 Hz, 6H). Not enough material was obtained to record a ^{13}C NMR, but the ^{1}H spectrum overlaps perfectly with *cis*-**3.3** obtained through photoisomerization and subsequent thermal helix inversion from *trans*-**3.3**.

3.8 References

1 K. Biradha, *CrystEngComm* **2003**, *5*, 374–384.
2 I. Weissbuch, M. Lahav, L. Leiserowitz, *Cryst. Growth Des.* **2003**, *3*, 125–150.
3 R. Bishop, *CrystEngComm* **2015**, *17*, 7448–7460.
4 K. M. Ok, *Acc. Chem. Res.* **2016**, *49*, 2774-2785.
5 Y. G. Huang, Y. Shiota, S. Q. Su, S. Q. Wu, Z. S. Yao, G. L. Li, S. Kanegawa, S. Kang, T. Kamachi, K. Yoshizawa, K. Ariga, O. Sato, *Angew. Chem. Int. Ed.* **2016**, *55*, 14628–14632.
6 K. N. Olafson, R. Li, B. G. Alamani, J. D. Rimer, *Chem. Mater.* **2016**, *28*, 8453-8465.
7 K. T. Mahmudov, M. N. Kopylovich, M. F. C. Guedes da Silva, A. J. L. Pombeiro, *Coord. Chem. Rev.* **2016**, 10.1016/j.ccr.2016.09.002.
8 P. Ball, *Nature* **1996**, *381*, 648–650.
9 The Cambridge Structural Database, https://www.ccdc.cam.ac.uk/solutions/csd-system/components/csd/.
10 J. -M. Lehn *Proc. Natl. Acad. Sci. U. S. A.* **2002**, *99*, 4763–4768.
11 J. Li, P. Nowak, S. Otto, *J. Am. Chem. Soc.* **2013**, *135*, 9222–9239.
12 Y. Jin, C. Yu, R. J. Denman, W. Zhang, *Chem. Soc. Rev.* **2013**, *42*, 6634–6654.
13 *Molecular Switches*, B. L. Feringa, W. R. Browne, Eds., Wiley-VCH Verlag GmbH & Co. KGaA: Weinheim, Germany, 2011.
14 S.-L. Huang, T. S. A. Hor, G.-X. Jin, *Coord. Chem. Rev.* **2016**, 10.1016/j.ccr.2016.06.009.
15 M. Morimoto, M. Irie, *Chem. Commun.* **2005**, 3895–3905.
16 E. R. Draper, D. J. Adams, *Chem. Commun.* **2016**, *52*, 8196–8206.
17 G. K. Kole, J. J. Vittal, *Chem. Soc. Rev.* **2013**, *42*, 1755–1775.
18 S. Ohshima, M. Morimoto, M. Irie, *Chem. Sci.* **2015**, *6*, 5746–5752.
19 Y.-N. Gong, T.-B. Lu, *Chem. Commun.* **2013**, *49*, 7711–7713.
20 B. L. Feringa, *J. Org. Chem.* **2007**, *72*, 6635–6652.
21 S. Kassem, T. van Leeuwen, A. S. Lubbe, M. R. Wilson, B. L. Feringa, D. A. Leigh, *Chem. Soc. Rev.* **2017**, *46*, 2592–2621.
22 R. Eelkema, M. M. Pollard, J. Vicario, N. Katsonis, B. S. Ramon, C. W. M. Bastiaansen, D. J. Broer, B. L. Feringa, *Nature* **2006**, *440*, 163.
23 E. R. Kay, D. A. Leigh, F. Zerbetto, *Angew. Chem. Int. Ed.* **2007**, *46*, 72–191.
24 D. J. van Dijken, J. Chen, M. C. A. Stuart, L. Hou, B. L. Feringa, *J. Am. Chem. Soc.* **2016**, *138*, 660–669.

25 S. J. Wezenberg, M. Vlatkovic, J. C. M. Kistemaker, B. L. Feringa, *J. Am. Chem. Soc.* **2014**, *136*, 16784–16787.
26 S. J. Wezenberg, C. M. Croisetu, M. C. A. Stuart, B. L. Feringa, *Chem. Sci.* **2016**, *7*, 4341–4346.
27 S. J. Grabowski, *Crystals* **2016**, *6*, 59.
28 K. E. Maly, E. Gagnon, T. Maris, J. D. Wuest, *J. Am. Chem. Soc.* **2007**, *129*, 4306–4322.
29 P. Li, O. Alduhaish, H. D. Arman, H. Wang, K. Alfooty, B. Chen, *Cryst. Growth Des.* **2014**, *14*, 3634–3638.
30 P. J. Langley, J. Hulliger, *Chem. Soc. Rev.* **1999**, *28*, 279–291.
31 M. A. Keniry, E. A. Owen, R. H. Shafer, *Nucleic Acids Res.* **1997**, *25*, 4389–4392.
32 Y. Zeng, Y. Pratumyot, X. Piao, D. Bong, *J. Am. Chem. Soc.* **2012**, *134*, 832–835.
33 Y. Wang, B. Wei, Q. Wang, *J. Crystallogr. Spectrosc. Res.* **1990**, *20*, 79–84.
34 C. T. Seto, G. M. Whitesides, *J. Am. Chem. Soc.* **1990**, *112*, 6409–6411.
35 C. T. Seto, G. M. Whitesides, *J. Am. Chem .Soc.* **1993**, *115*, 905–916.
36 B. Roy, P. Bairi, A. K. Nandi, *RSC Adv.* **2014**, *4*, 1708–1734.
37 T. M. Neubauer, T. van Leeuwen, D. Zhao, A. S. Lubbe, J. C. M. Kistemaker, B. L. Feringa, *Org. Lett.* **2014**, *16*, 4220–4223.
38 D. Zhao, T. M. Neubauer, B. L. Feringa, *Nat. Commun.* **2015**, *6*, 6652.
39 M. Numata, K. Sugiyasu, T. Kishida, S. Haraguchi, N. Fujita, S. M. Park, Y. J. Yun, B. H. Kim, S. Shinkai, *Org. Biomol. Chem.* **2008**, *6*, 712–718.
40 J. Coste, D. Le-Nguyen, B. Castro, *Tetrahedron Lett.* **1990**, *31*, 205–208.
41 D. L. Narayanan, R. N. Saladi, J. L. Fox, *Int. J. Dermatol.* **2010**, *49*, 978–986.
42 A. S. Lubbe, *A thymine functionalized molecular motor*, MSc Research Project Report, University of Groningen, 2012.
43 Q. Li, G. Fuks, E. Moulin, M. Maaloum, M. Rawiso, I. Kulic, J. T. Foy, N. Giuseppone, *Nat. Nanotechnol.* **2015**, *10*, 161–165.